OSCAR prototype station

Handbook of instrument

Authors: Francesco Amato, Marco Rosoldi, and Fabio Madonna

Contents

Figure

Tables

General Overview

The main target of the project is the development of an integrated system of measurement for the observation from the ground of atmospheric parameters of interest for climate variability on a regional scale. The project aims to provide a methodology to assess the relationship between climatic variables and the amount of radiation to the ground. This will allow, through an increase in the system of knowledge, to support actions aimed at strengthening the system of environmental monitoring networks and territorial, which increase energy efficiency and the protection and preservation of the natural heritage of Basilicata, in line with the strategies OP-ERDF 2007-2013.
Specific targets of the project are:

- Implementation of a low-cost integrated system prototype for the quantification of the impact of climate variability on the amount of radiation to the ground.
- Development of a methodology for estimating the impact of climate variability on the amount of radiation to the ground using the integration of the observations of the prototype measurement.
- Study of correlation between the radiation to the ground and precipitation events with extreme natural events and transport of aerosols.

Contacts

Mentor

Fabio Madonna, PhD
Istituto di Metodologie per l'Analisi Ambientale - Consiglio Nazionale delle Ricerche
CNR-IMAA
C.da S. Loja - Zona Industriale I-85050 Tito Scalo Potenza (Italy)
Phone: +390971427252
Fax: +390971427271
E-mail: fabio.madonna@imaa.cnr.it

Marco Rosoldi, PhD
Istituto di Metodologie per l'Analisi Ambientale - Consiglio Nazionale delle Ricerche
CNR-IMAA
C.da S. Loja - Zona Industriale I-85050 Tito Scalo Potenza (Italy)
Phone: +390971427250
Fax: +390971427271
E-mail: marco.rosoldi@imaa.cnr.it

Francesco Amato
Istituto di Metodologie per l'Analisi Ambientale - Consiglio Nazionale delle Ricerche
CNR-IMAA
C.da S. Loja - Zona Industriale I-85050 Tito Scalo Potenza (Italy)
Phone: +390971427261
Fax: +390971427271
E-mail: francesco.amato@imaa.cnr.it

Instrument Developers

Barometric Pressure Sensor CS106
Campbell Scientific, Inc.
815 West 1800 North
Logan, Utah 84321-1784
Phone: 435-753-2342
Fax: 435-750-9540
E-mail: info@campbellsci.com
Web: http://campbellsci.com

Gps Antenna Receiver SMART6-L
NovAtel, Inc.
1120 - 68 Avenue NE
Calgary, AB
Canada, T2E 8S5
Phone: +1-403-295-4500
Fax: +1-403-295-4901
E-mail: support@novatel.ca
Web: http://www.novatell.com

Rain Gauge Sensor RG13H
Vaisala
Vanha Nurmijärventie 21
FIN-01670 Vantaa
Finland
Phone: +358 9 8949 1
Fax: +358 9 8949 2227
E-mail: helpdesk@vaisala.com
Web: http://www.vaisala.com

HygroClip 2 (HC2) Humidity Temperature Probes
ROTRONIC AG
Grindelstrasse 6,
CH-8303 Bassersdorf
Phone: + 41 44 838 11 11
Fax: + 41 44 838 14 83
E-mail: info@rotronic.ch
Web: http://www.rotronic.com/

SMP3 Pyranometer
Kipp & Zonen B.V.
Delflechpark 36, 2628 XH Delft, Netherlands
Phone: +31 (0) 15 2755 210
Fax: +31 (0) 142620 351
E-mail: support@kippzonen.com
Web: http://www.kippzonen.com

Arduino Mega 2560 microcontroller board
Arduino
Web: https://www.arduino.cc

Deployment Location and History

The project has been carried out at the CNR-IMAA Atmospheric Observatory), named CIAO (Madonna et al., 2011), which is a leading research center for the study of the atmosphere. The project makes use of historical observations made at CIAO with ground-based equipment for the study of the atmosphere.

Table 1 - Location and History

Location	Date Installed	Date Removed	Status
CIAO, PZ			operational

Near-Real-Time Data Plots

Near-Real-Time Data Plots can be found at the following locations:
http://www.ciao.imaa.cnr.it/index.php?option=com_content&view=article&id=188&Itemid=256

Data Description and Examples

Primary Variables and Expected Uncertainty

Table 2 - Primary Variables

Quantity	Variable	Unit	Resolution
Temperature	temp	°C	0.01
Pressure	press	hPa	0.1
RH	rh	%	0.1
Precipitation	precip	mm	0.001
Radiance	rad	W/m²	0.1
Integrated PrecipiTable Water Vapour	ipwv	cm	0.001

Instrument Details

Detailed Description

List of Components

Barometric Pressure sensor

The CS106 analog barometer uses Vaisala Barocap silicon capacitive pressure sensor. The Barocap sensor has been designed for accurate and stable measurements of barometric pressure. The CS106 outputs a linear 0 to 2.5 VDC signals that corresponds to 500 to 1100 mb. It can be operated in a shutdown or normal mode. In the shutdown mode the datalogger switches 12 VDC power to the barometer during the measurement. The datalogger then powers down the barometer between measurements to conserve power.

Figure 1 - Vaisala Pressure sensor CS106

The pressure value can be retrieved using equation below.

$$T = 500 + 120 * V_{out}[hPa]$$

T/RH sensor

HC2 Rotronic series are digital humidity-temperature probes based on the AirChip 3000 technology. These probes feature a UART serial interface and two 0…1 V linear analog output signals. The HC2 probes are designed for use with the HygroClip 2 generation of Rottronic humidity-temperature instruments: hand-held and bench top indicators, data loggers, transmitters, hygrostats, etc. The HC2 probes maintain all of the benefits of the original HygroClip technology such as the possibility of hot-swapping probes and feature significant improvements in the area of measurement accuracy and functionality. The HC2 probes can also be used as a stand-alone device using either the analog output signals or the probe digital interface. Connectors, cables and digital interface adapters are available to this purpose. Digital integration with OEM applications is facilitated by the probe communication protocol options.

Figure 2 - HC2 Rotronic Temperature/Relative Humidity sensor

The temperature and relative humidity values can be retrieved using equations below:

$$T = -40 + 100 * V_{out}[°C]$$

$$RH = 100 * V_{out}$$

Precipitation

Vaisala Rain Gauge RG13 has a body and funnel of aluminum alloy, with an accurately machined septum-ring at the top to give an orifice of 400 cm2. Bucket mechanism is mounted inside the body on a cast aluminum-alloy base incorporating fixing lugs, three leveling screws, and a spirit level. The rain gauge comprises a divided bucket assembly, which is pivoted at its center like a seesaw. Rain collects in the upper half of the bucket, The RG13H heated tipping bucket type rain gauge provides a well proven and reliable method of monitoring rainfall also at temperatures below 0 °C. RG13H is equipped with the internal heater. The heater switches on at temperatures below +4 °C. The heater power consumption is 38 W/40 VDC. which is adjusted to tilt when a predetermined amount of water has been collected. The tilting action discharges the collected water, and repositions the opposite half under the discharge nozzle ready for filling. The bucket tips are monitored by means of a magnet, which energizes a reed switch capable of a virtually indefinite amount of operations. This system ensures that the tipping bucket has a long, reliable working life.

Radiance sensor

The SMP series instruments are high quality radiometers designed for measuring short-wave irradiance on a plane surface (radiant flux, W/m²), which results from the sum of the direct solar radiation and the diffuse sky radiation incident from the hemisphere above the instrument. SMP pyranometers feature internal digital signal processing and interfaces optimized for industrial data acquisition and control systems. Kipp & Zonen has developed a smart interface that features RS-485 Modbus® data communication for connection to programmable logic controllers (PLC's), inverters, digital control equipment and the latest generation of data loggers. Amplified Voltage or Current outputs are also included for devices that have high-level analogue inputs or current loop interfaces. Digital signal processing provides faster response times and, with an integrated temperature sensor, corrects for the temperature dependence of the detector sensitivity.
The irradiance value for the default setting can be simply calculated as shown below:

$$I = -200 + 2200 * V_{out}[W/m^2]$$

Figure 3 - Vaisala Rain Gauge RG13

Figure 4 - Kipp & Zonen SMP pyranometer

GPS Antenna/Receiver

The SMART6-L is a high performance GNSS receiver and antenna, capable of receiving and tracking different combinations of GNSS L1/L2 code and carrier signals on a maximum of 120 channels. SBAS (Satellite Based Augmentation Systems) includes WAAS (North America), EGNOS (Europe) and MSAS (Japan). SBAS support is standard. Refer to NovAtel's GNSS Book for an overview of each of the above signal types. The SMART6-L rear panel also features Light Emitting Diodes (LEDs) for status indication. Once properly powered, the SMART6-L begins operating as a fully functional GNSS system.

Figure 5 - Novatel SMART6-L Antenna

A constellation of GPS satellites transmit atomic-clock controlled *L-band* signals to GPS receivers on the ground. Data recorded by GPS receivers at fixed locations will show *signal path delays* caused by a variety of effects. One class of GPS-signal delays can be directly attributed to the passage of the signals through the Earth's ionosphere and atmosphere.

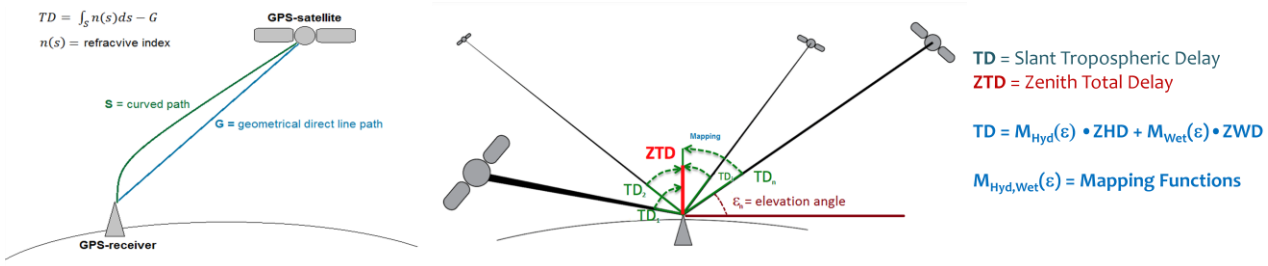

Figure 6 – GPS tropospheric delay evaluation

The *ionospheric delay* can be eliminated by using a dual-band GPS receiver. The remainder of the atmospheric delay, or the ***total tropospheric delay***, can be decomposed into a *"**hydrostatic delay** (HD)"* associated with induced dipole moment of the dry atmosphere and a *"**wet delay** (WD)"* associated with the permanent dipole moment of water vapor. The hydrostatic delay accounts for nearly 90% of the total tropospheric delay, and can be estimated with an accuracy of 0.2% from surface meteorological data. The total tropospheric delay measured by a GPS receiver is eventually mapped to the ***Zenith Total Delay** (ZTD)* using a mapping function. Saastamoinen showed (Saastamoinen J., 1972) that the ZTD can be expressed as the sum of Zenith Hydrostatic Delay (ZHD) and the Zenith Wet Delay (ZWD). The ZTD is one of the parameters that is routinely

estimated by the GPS analysis software, together with other parameters such as coordinates, satellite-receiver clock errors, and phase ambiguity parameters. The ZWD can be estimated by subtracting ZHD from the ZTD where the ZHD is derived from the surface pressure , temperature, and humidity. The ZWD then can be converted into an estimate of IPWV:

$$IPWV = \pi * ZWD[cm]$$

Data gathered by a *Novatel GPS antenna* are locally processed using a software developed at CIAO. The Mapping functions used to retrieve the tropospheric delay are the Niell, Saastamoinen, Chao and Herring Mapping Functions, while the Saastamoinen model has been used in order to evaluate the hydrostatic delay.

Data logger

The Arduino Mega 2560 is a microcontroller board based on the ATmega2560. It has 54 digital input/output pins (of which 15 can be used as PWM outputs), 16 analog inputs, 4 UARTs (hardware serial ports), a 16 MHz crystal oscillator, a USB connection, a power jack, an ICSP header, and a reset button. It contains everything needed to support the microcontroller; simply connecting it to a computer with a USB cable or power it with a AC-to-DC adapter or battery to get started. The Mega is compatible with most shields designed for the Arduino Duemilanove or Diecimila. The Mega2560 differs from all preceding boards in that it does not use the FTDI USB-to-serial driver chip. Instead, it features the ATmega16U2 (ATmega8U2 in the revision 1 and revision 2 boards) programmed as a USB-to-serial converter.

Figure 7 - Arduino Mega 2560 board

Each of the 54 digital pins on the Mega can be used as an input or output, using *pinMode()*, *digitalWrite()*, and*digitalRead()* functions. They operate at 5 volts. Each pin can provide or receive a maximum of 40 mA and has an internal pull-up resistor (disconnected by default) of 20-50 kOhms. The Mega2560 has 16 analog inputs, each of which provide 10 bits of resolution (i.e. 1024 different values). By default they measure from ground to 5 volts, though is it possible to change the upper end of their range using the AREF pin and *analogReference()* function.

Within this context the Arduino board has been used in order to log and records data over time of Pressure, Temperature, RH, Irradiance and Precipitation sensors.

Lidar System: SOLIS

Lidar System

The lidar system SOLIS (Scanning OSCAR LIdar System) is based on a 20 Hz Nd:YAG laser source, a Big Sky Quantel CFR 200 Model series, emitting light pulses at 532 nm. The laser is powered, controlled and cooled by a mobile Quantel substation model ICE (Integrated Cooler and Electronics). The essential parts of the laser transmitter are shown in Figure 8.

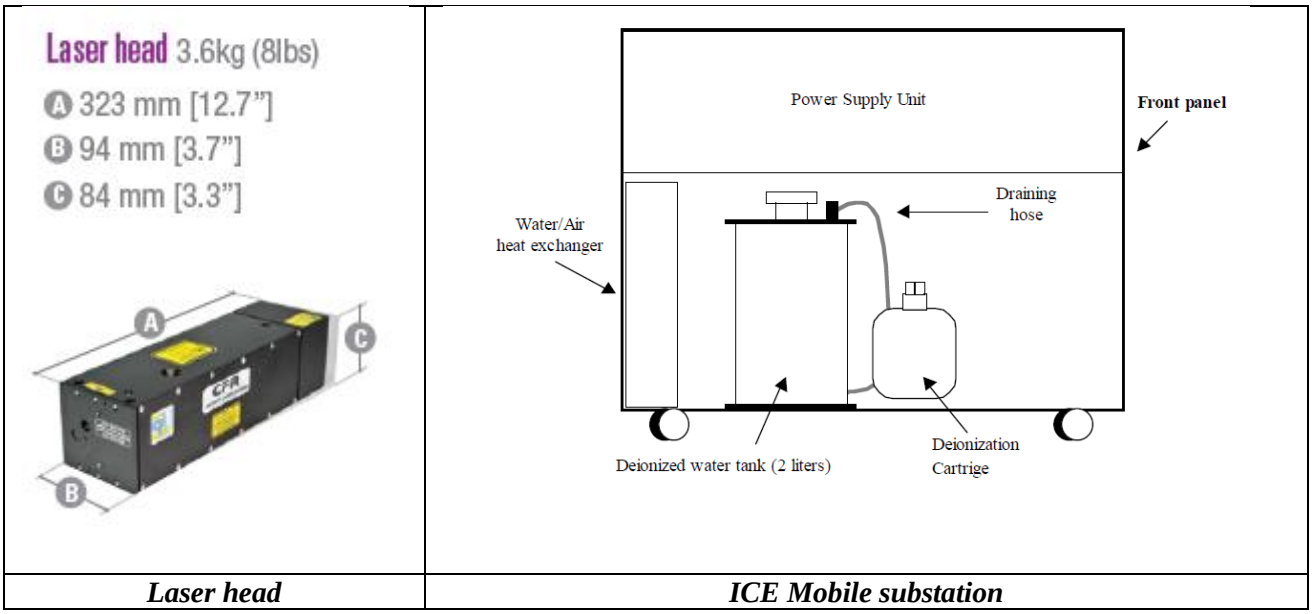

Laser head	*ICE Mobile substation*

Figure 8 - Big Sky Quantel Laser

The laser beam passes through a beam expander (10X) with the aim to make eye safe the system, by reducing the laser beam power, and to reduce the laser beam divergence. The beam outgoing from the expander is transmitted into the atmosphere coaxially with respect to the lidar receiver, by means of a pair of mirrors. The lidar receiver is a f/4 Newton telescope with a primary mirror of 150 mm diameter, an equivalent focal length of 600 mm and a carbon fiber intubation, produced by the German firm Telescope Service (TS), model UNC1506 (Figure 9). In addition, the telescope is equipped with a cooling fan for thermal stabilization of the primary mirror. The optical and mechanical features of the telescope are detailed in Figure 10.

The backscattered radiation from the atmosphere is collected by the telescope and forwarded to the receiving system by means of an optical system consisting of a mirror, an interference filter and a beam splitter. The receiving system is equipped with 3 channels. One of these is devoted to the detection of the elastically backscattered radiation from the atmosphere at 532 nm. The other two channels detect the polarized components of the elastically backscattered radiation at 532 nm, with polarization perpendicular (S) and parallel (P) with respect to the polarization of the linearly polarized beam transmitted by the laser, by means of a polarizing beam splitter cube. For each acquisition channel, the detection is performed by a photomultiplier tube and the acquisition is performed both in analog and photon counting mode, in order

to increase the detectable dynamic range of lidar signals. The output signal of the photomultiplier is split in two components: a component is sent to an Analog to Digital Converter (ADC), whose output represents the analog signal, while the other component is sent to a counting system (a discriminator plus a counter), whose output represents the photon counting signal.
This lidar allows measurements of particle backscattering coefficient and linear depolarization ratio at 532 nm. The calibration of depolarization channels is made by performing consecutive measurements with polarizations of ± 45° with respect to the direction of incident polarization. The rotation of polarization is achieved by a linear polarizer, placed before the polarizer cube, which can rotate of ±45° with respect to a fixed position. Further linear polarizers are placed along the reflection and transmission channels of the polarizer cube in order to minimize the cross talk components outgoing from the cube (residuals of P component in the transmission channel S and of S component in the reflection channel P).
The optical configuration of the lidar system is given in Figure 11, while the main specifications are listed in Table 3.

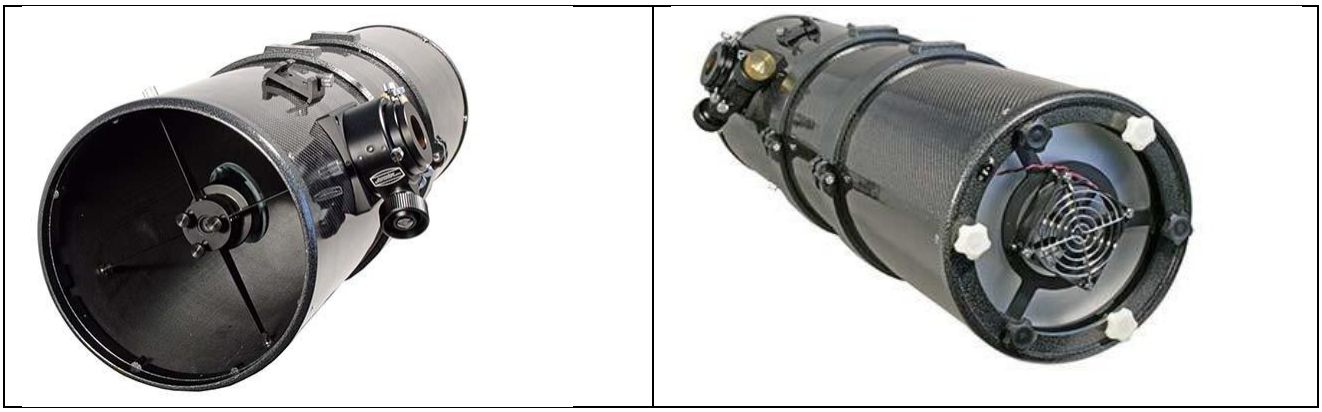

Figure 9 - TS UNC1506 telescope

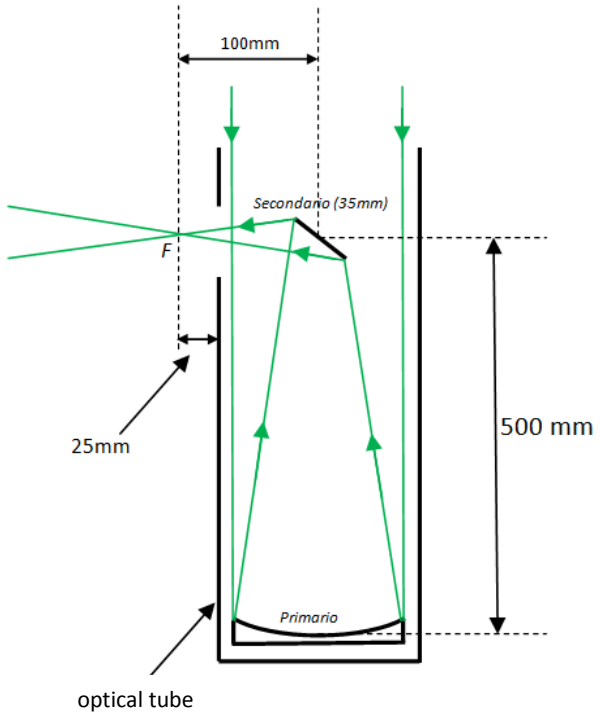

Legend:
Primary parabolic mirror diameter: 150 mm
Secondary elliptical mirror Minor axis: 35 mm
Secondary elliptical mirror Major axis: 1.41 X 35 mm = 49.5 mm
Focal length: 600 mm
F: focus
Distance of F from the optical tube: 25 mm
Distance of F from the secondary mirror: 100 mm
Distance between the secondary mirror and the primary mirror: 500 mm
Weight of optical tube: 4 kg

Figure 10 - Telescope technical features

Legend:
M: Mirror
PH: Pin Hole
L: Lens
IF: Interferential Filter
BS: Beam Splitter
RLP: Rotating Linear Polarizer
PBS: Polarizing Beam Splitter
LP-s: Linear polarizer: cross component
LP-p: Linear polarizer: parallel component
PMT: photomultiplier

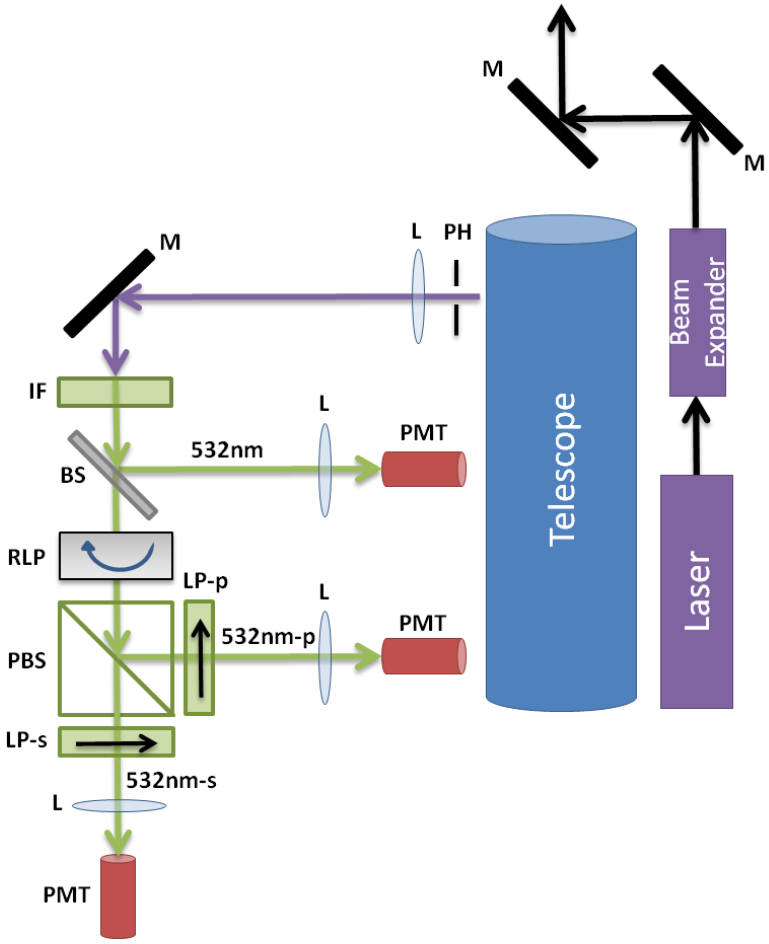

Figure 11 – Optical Layout of the lidar system

Table 3 - Main specifications of lidar system

Emitter						
Pulsed laser Source	Nd:YAG (Quantel CFR 200 Series)					
Laser Class	IV					
Wavelength	532 nm					
Energy per Pulse	130 mJ					
Repetition Rate	20Hz					
Laser Beam Diameter (Near Field)	< 6.35mm					
Laser Beam Divergence (Full Angle)	< 0.8 mrad					
Beam Expander	5X					
Beam Divergence	2.5 mrad (tunable from 1.5 to 3mrad)					
Receiver						
Telescope Configuration	Newton					
Primary Mirror Diameter	150 mm					
Minor Axis of Secondary Mirror	35 mm					
F/ Number	F/4					
Focal length	600 mm					
Field Of View	2.5 mrad (tunable from 1.5 to 5 mrad)					
Detection and Channel Selection						
Elastic Backscattering	532nm P (Parellel)				Photoncounting	
	532nm S (Cross)				Photoncounting	
Elastic Backscattering	532nm (Total)				Photoncounting	
Interferential filter	Central wavelength 532 nm				Bandwidth 0.5 nm	
Polarizer Beam Splitter Cube (BK7)	Wavelength 532nm					
Photomultipliers (Hamamatsu)						
Type	**Luminous Sensitivity Cathode (µA/lm)**		**Luminous Sensitivity Anode (A/lm)**		**Dark Anode (nA)**		**Input Voltage**
	Min	**Typ**	**Min**	**Typ**	**Typ**	**Max**	
H10721P-110	80	105	80	210	1	10	4.5-5.5V
H10721P-110	80	105	80	210	1	10	4.5-5.5V
H10721P-110	80	105	80	210	1	10	4.5-5.5V

Steering unit

The lidar system is mounted on a plate and can be rotated on a vertical plane, so as to transmit the laser beam to the sky and detect the backscattered radiation from the atmosphere within a scanning angle of +/- 30° with respect to the zenith direction, as shown schematically in Figure 12. This configuration allows to measure the profiles of particle backscattering coefficient and linear depolarization ratio within that scanning angle.

The lidar scanning is performed by using a motorized rotary stage 100 mm in diameter, the AGR 100 - BMS model with Direct Encoder, driven by a controller ENSEMBLE MP10 with Ethernet interface and related software, produced by US company Aerotech (Figure 13). The rotational stage base is fabricated from an

aluminum alloy that offers significant weight savings in multi-axis arrangements and other weight critical applications, while providing high structural stiffness and long-term stability. The stage features an Aerotech's brushless DC servomotor.

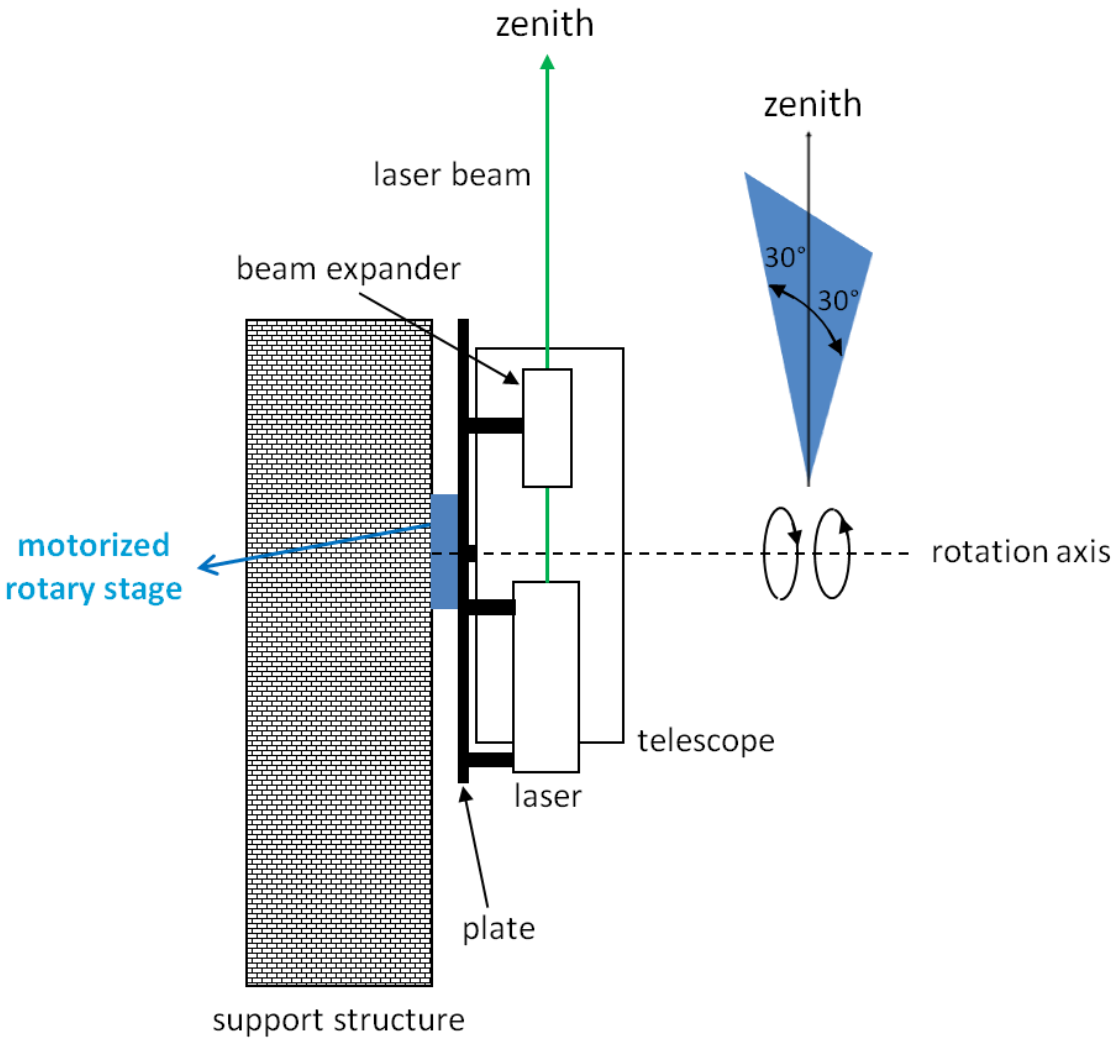

Figure 12 – Lidar system rotating on a vertical plane within ±30° with respect to the zenith direction

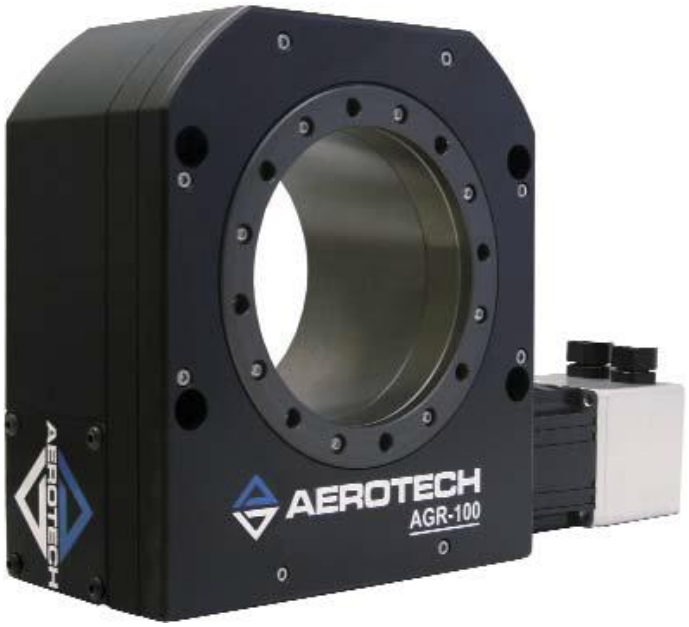

Figura 13 – Aerotech's rotary stage AGR 100 – BMS with Direct Encoder

The load capacity of the AGR 100 rotary stage as a function of distance from the rotation axis (axial) and from the rotation tabletop/shaft (radial) is shown in Figure 14.

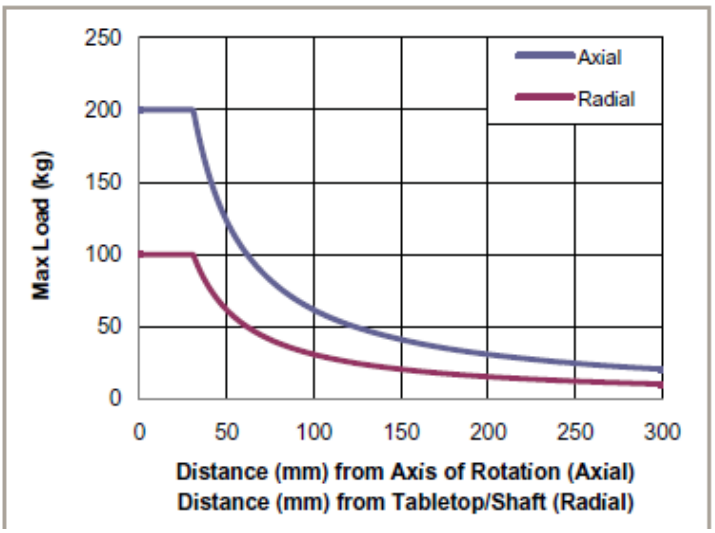

Figura 14 - Axial (violet line) and radial (red line) cantilevered load capability for AGR 100 rotary stage

The mechanical and geometrical specifications of the AGR 100 – BMS rotary stage with Direct Encoder are reported in Table 4 and Figure 15, respectively.

Table 4 - Mechanical specifications of Aerotech rotary stages - AGR series

Mechanical Specifications		AGR50	AGR75	AGR100	AGR150	AGR200
Travel		360° (Limited Travel Versions Available)				
Accuracy[1]	Standard	180 arc sec		120 arc sec		
	Direct Encoder	20 arc sec				
Repeatability (Uni-Directional)[1]	Standard	10 arc sec				
	Direct Encoder	5 arc sec				
Repeatability (Bi-Directional)[1]	Standard	45 arc sec				
	Direct Encoder	8 arc sec				
Tilt Error Motion		10 arc sec				
Axial Error Motion		5 µm				
Radial Error Motion		10 µm				
Gear Ratio		51:1	67:1	85:1	117:1	126:1
Maximum Speed[2]	BM/BMS	180°/s				120°/s
	SM	60°/s		40°/s		
Maximum Acceleration[3]		720°/s²				480°/s²
Aperture	mm	50 mm	75 mm	100 mm	150 mm	200 mm
Load Capacity	Axial	40 kg	100 kg	200 kg	300 kg	425 kg
	Radial	20 kg	50 kg	100 kg	125 kg	200 kg
	Moment	See Moment Load Curves				
Maximum Torque Load to Stage Shaft		2.5 N·m	3.5 N·m	12 N·m	20 N·m	80 N·m
Rotor Inertia (Unloaded)		0.00052 kg·m²	0.0013 kg·m²	0.0035 kg·m²	0.011 kg·m²	0.076 kg·m²
Stage Mass (No Motor)	Standard	1.9 kg	2.4 kg	4.5 kg	6.1 kg	18.6 kg
	Direct Encoder	2.5 kg	3.1 kg	5.6 kg	7.6 kg	21.7 kg
Material		Aluminum				

Note:
1. Certified with each stage.
2. Maximum speed is load dependent. Contact an Aerotech Application Engineer if imbalanced loads are present.
3. Unloaded acceleration.
4. On-axis loading is listed.
5. Specifications are for single-axis systems measured 25 mm above the tabletop. Performance of multi-axis systems is payload and workpoint dependent. Consult factory for multi-axis or non-standard applications.

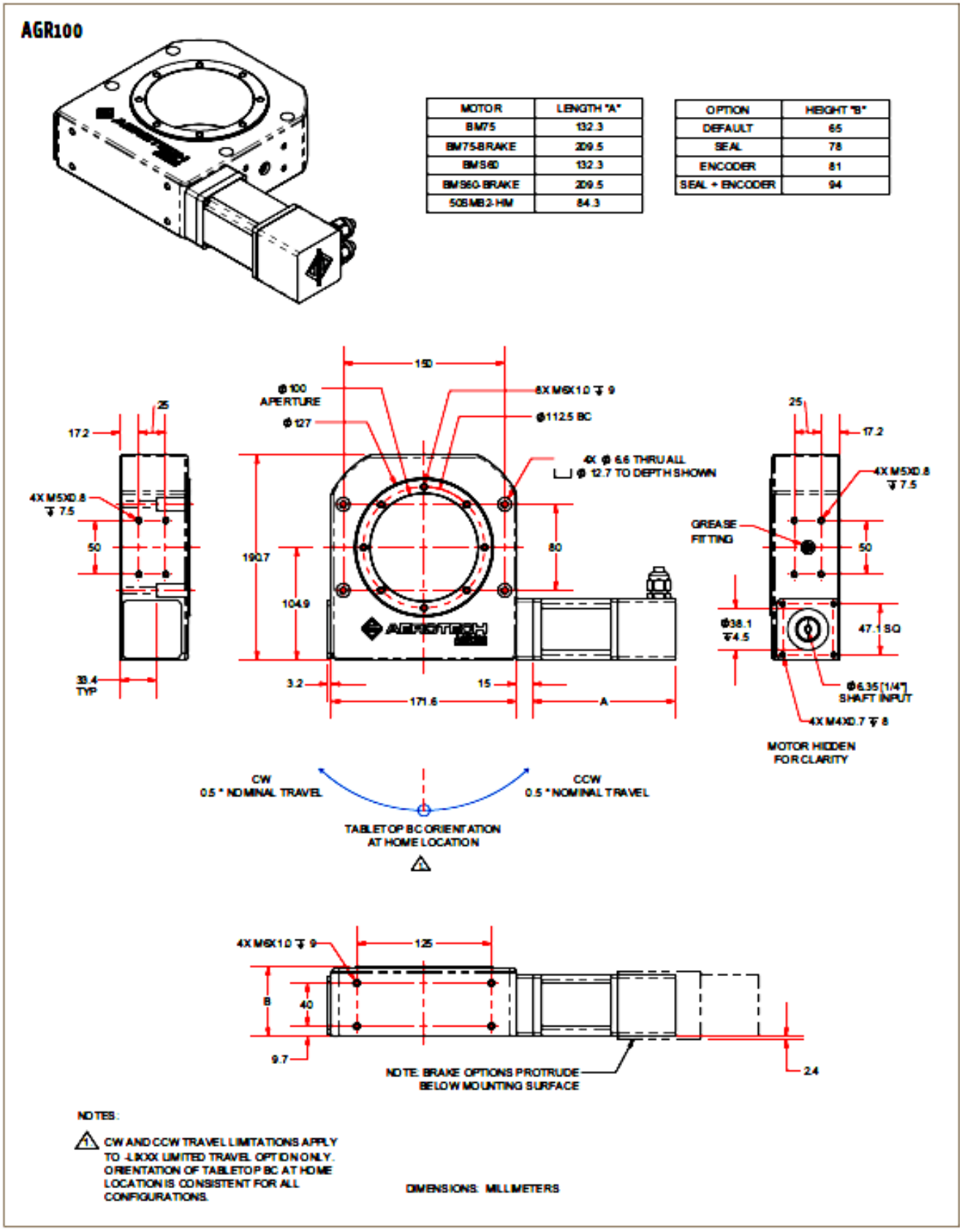

Figure 15 – Geometrical specifications of the AGR 100 – BMS Standard model rotary stage

The ENSEMBLE MP 10 controller is powered continuously with a 80V/5A bench supply. The technical specifications of the controller are shown in Table 5.

Table 5 - Ensemble MP specifications

Ensemble MP
Width: 41.1 mm
Height: 141.2 mm

Ensemble MP	Units	
Motor Style		Brush, Brushless, Stepper(1)
Motor Supply	VDC	10-80
Control Supply(2)	VDC	24-80
Bus Voltage(3)	VDC	10-80
Peak Output Current (1 sec)(4)	A_{pk}	10
Continuous Output Current(4)	A_{pk}	5
Digital Inputs	—	N/A
Digital Outputs	—	N/A
Analog Inputs	—	One 16-bit Differential; ±10 V
Analog Outputs	—	N/A
Dedicated Axis I/O on Feedback Connector		Three Limit Inputs (CW, CCW, Home); Three Hall Effect Inputs (A, B, C); Three High-Speed differential Inputs (sin, cos, mkr for encoder); Motor Over-Temperature Input
Dedicated I/O on Auxiliary Feedback Connector		N/A
I/O Expansion Board(5)	—	8/8 Digital Opto-Isolated; 1 Analog In (±10 V, 12-bit Differential); 1 Analog Out (±5 V, 16-bit); sin, cos, mkr for Aux Enc; Aux Enc can be used for PSO Output
High Speed Data Capture		Yes (50 ns Latency)
Automatic Brake Control	—	Optional(5)
Emergency Stop Sense Input (ESTOP)(6)	—	Standard; 24 V Opto-Isolated
Position Synchronized Output (PSO)	—	Optional(5)
Can Output Multiplied Encoder		No
Can Output Square Wave Encoder		Yes
Primary Encoder Input Frequency		200 kHz Amplified Sine Wave Standard (for onboard multiplier); 40 MHz TTL Square Wave
Secondary Encoder Input Frequency		32 MHz Square Wave
Encoder Multiplication	—	Up to x4096 (MXU)
Resolver Interface	—	N/A
Internal Shunt Resistor		N/A
External Shunt		N/A
Ethernet	—	Yes
USB		No
RS-232		Yes
FireWire		No
Fieldbus		Modbus TCP; Ethernet/IP
Current Loop Update Rate	kHz	20
Servo Loop Update Rate	kHz	1 to 20
Power Amplifier Bandwidth	kHz	Selectable Through Software
Minimum Load Inductance	mH	0.1 @ 80 VDC
Operating Temperature	°C	0 to 50
Storage Temperature	°C	-30 to 85
Weight	kg (lb)	0.45 (1.0)

Notes:
1. For stepper motors only, one-half of bus voltage is applied across the motor (e.g., 80 VDC supply results in 40 VDC across stepper motor).
2. "Keep Alive" supply.
3. Output voltage dependent upon input voltage.
4. Peak value of the sine wave; rms current for AC motors is 0.707 * A_{pk}.
5. Requires IO option.
6. Requires external relay to remove motor supply power.

Lidar calibration

The correct operation of the lidar system is ensured by specific tests developed in the frame of EARLINET/ACTRIS quality assurance program (Pappalardo et al., 2014). These tests aim to measure the experimental parameters to be used in the pre-processing of lidar data in order to correct possible biases and to identify possible distortions in lidar signals. The lidar calibration is obtained by performing the following tests, with the lidar in zenith pointing configuration:

- *Trigger delay and first bin range measurement*

In lidar systems the acquisition electronics receives a trigger signal synchronous to the emissions of laser pulses. In this way, lidar signals are acquired where the first bin coincides with the instant of emission of each laser pulse, in the time domain, and with the zero altitude, in the spatial domain. All subsequent altitudes of lidar profile are calculated starting from this zero altitude.

Both the electronics of the acquisition system and the electronics for the transmission of the trigger signal to the acquisition system can cause a discrepancy between the instant of emission of a laser pulse and the start of the acquisition related to that laser pulse. Two different situations may occur. In the first, the start of the acquisition is delayed compared to the instant of emission of the laser pulse and the discrepancy, called *trigger delay*, results in an underestimation of the altitudes in lidar signal. In the second, the start of the acquisition is in advance compared to the instant of emission of the laser pulse and the discrepancy, called *first range bin*, results in an overestimation of the altitudes in lidar signal.
Both *trigger delay and first range bin* lead to errors not only in the determination of the altitudes from which the lidar signal comes, but also in calculating the optical parameters during the subsequent analysis of lidar signals. Therefore, for each acquisition channel the above discrepancy, that is the time interval between the emission of laser pulse and the start of acquisition, must be accurately measured, in order to correct the corresponding lidar signals.

- *Dead time measurement*

Each acquisition system in photon counting mode, consisting of a photomultiplier tube, a discriminator and a pulse counter, is characterized by a time interval during which the system is unable to count incident photons. This time interval is called dead time. If two photons arrive at the photocathode of the photomultiplier in a time interval less than the dead time, the acquisition system records a single count. As a result, the acquisition in photon counting mode is characterized by a maximum count rate above which the observed count rate is no more proportional to the number of photons arriving at photocathode but depends on the dead time duration. Therefore, for each acquisition channel in photon counting mode the dead time must be accurately measured in order to correct the corresponding lidar signals so as to extend the linearity of the acquisition system up to high count rates.

- *Telecover test*

For each acquisition channel, the telecover test is performed by dividing the surface of the primary mirror of the telescope in different circular sectors with equal area and measuring the lidar signal coming from each sector (by obscuring all others). This measurements must be performed in very sTable atmospheric conditions to avoid variations for different sectors due to atmospheric variability. In this way, lidar signals generated by light beams passing through different portions of the receiving optics and incident on different regions of the photocathode of the photomultiplier can be measured. By comparing these signals, normalized in an altitude range where the atmosphere is stable, it is possible:

a) check the presence of distortions of lidar signals in the near range (planetary boundary layer);
b) estimate the height of full overlap between the laser beam and the field of view of the telescope
c) check and correct the alignment of the laser beam with the telescope in the near range.

- *Rayleigh fit test*

For each acquisition channel, the Rayleigh fit test is performed by comparing the lidar signal with a reference lidar signal, generated by a molecular atmosphere, in an aerosol free altitude range. The reference molecular lidar signal can be calculated from vertical profiles of atmospheric pressure and temperature, measured with a radiosounding or obtained from models or a standard atmosphere, by using the Rayleigh scattering theory (Bucholltz, 1995; Miles et al, 2001). With the Rayleigh fit test, it is possible:

a) check the presence of distortions of lidar signals in the far range (free troposphere or above);

b) check and correct the alignment of the laser beam with the telescope in the far range.

- *Dark measurements*

Lidar signals, as all the signals acquired with electronic devices, can be affected by electronic distortions not related to the light backscattered from the atmosphere and collected by the telescope. These distortions, mostly affecting the signals acquired in analog mode, can be removed or reduced by performing dark measurements, that is, by measuring the lidar signals for each acquisition channel with the telescope completely obstructed. These dark signals are not affected by the light backscattered from the atmosphere and contain only the electronic distortions. Therefore, by subtracting these dark signals from lidar signals the removal or a reduction of the electronic distortions in lidar signals can be obtained.

- *Calibration of polarization channels*

To make accurate measurements of depolarization, the calibration of polarization channels is needed. The polarizing beam splitter cube (PBS) reflects the parallel component and transmits the perpendicular component, with respect to the direction of polarization of the light transmitted by the laser. However, the parallel component of incident light on the cube can form an angle with respect to the optical axis of the cube, called offset angle. This produces cross-talk components in transmitted and reflected light from the cube. To minimize these components, the polarization of incident light on the cube is rotated by the offset angle, by rotating the linear polarizer placed before the cube.
The determination of the offset angle, and then of the correct measurement position of the rotating linear polarizer, is obtained by measuring the lidar signals P_S and P_P of perpendicular and parallel components, with the polarizer at + 45 ° and - 45 ° with respect to its starting position. Varying the starting position of the polarizer and measuring the lidar signals P_S and P_P with the polarizer at + 45 ° and - 45 ° with respect to that position, it is possible to determine and fix the zero-offset position of the polarizer as the position for which P_S (+ 45 °) = P_S (-45 °) and P_P (+ 45 °) = P_P (-45 °).
Fixed the zero-offset position of the polarizer, it is possible to measure the polarization factor. For this purpose, it is used the "±45° calibration" method discussed in (Freudenthaler et al., 2009). The ratio between the lidar signals P_S and P_P, acquired by the channels at 532nm-s and 532nm-p, with the polarizer in the zero-offset position, can be expressed as:

$$\eta(r) = \frac{P_S(r)}{P_P(r)} = \frac{g_\perp(r)}{g_\parallel(r)} \frac{\beta_\perp(r)}{\beta_\parallel(r)} = G\delta^V$$

where: r is the distance of atmospheric scatterers from the lidar; $G = g_\perp(r)/g_\parallel(r)$ is the depolarization gain ratio, depending on the optical efficiency of optics that light passes through (polarizing beam splitter cube, interferential filters, lenses, neutral density filters) and on the electronic efficiency of detectors; $\delta^V = \beta_\perp(r)/\beta_\parallel(r)$ is the volume depolarization ratio, defined as the ratio between the total backscattering coefficient (due to particles and molecules) related to the light component with polarization perpendicular to the polarization direction of the incident light and the total backscattering coefficient related to the light component with polarization parallel to the direction of incident polarization.
δ^V can be calculated from the ratio of the lidar signals η(r), known the gain G, whose inverse is the polarization factor C. This is calculated by measuring the lidar signals P_S and P_P, acquired by the channels at 532nm-s and 532-p, with the rotating polarizer at + 45 ° and - 45 ° with respect to the zero-offset position. In this case, we have:

$$\frac{1}{C} = G = \sqrt{\eta(+45°) \cdot \eta(-45°)}$$

The lidar measurements to calculate the polarization factor C must be performed in a temporal window with sTable and homogeneous atmospheric conditions. Because these conditions are rarely met in cloud or

aerosol layers, calibration measurements are typically performed in those regions that most resemble clear air. This clear air region need not be purely molecular; however, any aerosol background eventually present must be uniformly distributed, both spatially and temporally.
Once measured C, it is possible to return to the initial measurement configuration, with the rotating polarizer at the offset angle, and δ^V is calculated by the product between the ratio of the lidar signals η (r) and C.

Signal processing

This section describes the main instrumental corrections to be done on raw lidar signals before using them in the algorithms for the retrieval of aerosol optical properties. This stage of lidar analysis is commonly known as "pre-processing" of lidar data and represents a necessary step in the analysis of lidar data. The pre-processing of lidar signals is performed by the following steps:

- *Correction for atmospheric background*

Each lidar channel measures a signal which is the superposition of two contributions: the contribution of backscattered radiation from the atmosphere and the contribution of solar background. The former is range dependent, while the latter is range independent. In lidar analysis it is necessary to separate the two contributions and consider only the signal due to the backscattering from the atmosphere. Because this signal usually decreases with increasing range, it is possible to obtain the contribution of solar background, by averaging the measured signal on the far field range, where the signal due to the backscattering from the atmosphere can be neglected with respect to the solar background signal. Although the background signal can be subtracted from the measured signal, it limits the signal to noise ratio of lidar signals in daytime measurements.

- *Correction for electronic distorsions*

The electronic distortions mainly affect lidar signals acquired in analog mode. These signals are used in the analysis of lidar data only for low ranges, where lidar signals due to atmospheric backscattering are usually predominant with respect to any electronic distortion. On the other hand, in order to eliminate or reduce any residual distortion, during acquisition/pre-processing of lidar signals, the following procedure is performed:

1) Acquiring N dark signals for each channel, before performing ordinary lidar measurements
2) Averaging the N dark signals for each channel
3) Subtracting from the signal acquired with each channel the corresponding average dark signal obtained in the previous point

- *Correction for dead time*

All lidar signals in photon counting mode must be corrected for dead time effect so as to extend the linearity of the acquisition system up to high count rates.
There are two different models to describe a photon counting system: paralyzable model and not paralyzable one. A paralyzable system is unable to record a second output pulse unless there is a time interval of at least the dead time τ between two successive input pulses. If an additional pulse arrives during the response time, the dead time of the system is further extended by τ. For high count rate, the system is not able to respond and it remains completely paralyzed, by providing a zero count rate. By using Poisson probability distribution, a paralyzable system is described by the following formula:

$$N_m = N_r \exp\left(-\tau N_r\right)$$

where N_m and N_r are the measured count rate and the real count rate, respectively.
In a not paralyzable system the dead time τ, or response time, is independent of the arrival of additional counts. For high count rate, the system asymptotically approaches a maximum count rate N_{max}, which is the inverse of dead time. A not paralyzable system is described by the following formula:

$$N_m = \frac{N_r}{1+\tau N_r}$$

The correction for dead time is performed by inverting one of the two previous equations with respect to the real count rate N_r , after accurate measurements of dead time for each photon counting channel.
Concerning the equation to be used, it is necessary to specify that real systems are never completely paralyzable or not paralyzable, but their behavior is somewhat intermediate between these two models. Therefore, none of the two previous equations correctly describes a real photon counting system. However, for measured count rates not too high, the two models produce very similar results and the choice between the two models becomes irrelevant.

- *Correction for trigger delay and first range bin*

The correction for trigger delay/first range bin is performed by interpolating the lidar signals to the correct times or ranges. Consider, for example, a lidar channel with spatial resolution of 15m, corresponding, in the time domain, to a dwell time of 100ns. Suppose also that the same channel is affected by a trigger delay/first range bin of ± dt. The raw uncorrected lidar signal of the channel is $S_{raw}=\{(t_1,s_1), (t_2,s_2),\ldots(t_n,s_n)\}$, where the instants t_i are 50, 150, 250,…ns, corresponding, in the range domain, to 7.5, 22.5, 37.5,…m. Because the channel is affected by a trigger delay/first range bin of ± dt, the measured intensities $s_1, s_2,\ldots s_n$ refer to the instants $t_1\pm dt$, $t_2\pm dt,\ldots t_n\pm dt$ and not to the instants $t_1,t_2,\ldots t_n$. As a consequence, the correct association between measured intensities and times-range bins is $S_{corr}=\{(t_1\pm dt,s_1), (t_2\pm dt,s_2),\ldots(t_n\pm dt,s_n)\}$.
Because it is convenient to express the lidar signal in terms of the instants t_i, the signal S_{corr} is interpolated to the instants t_i.

- *Gluing between analog signals and photon counting signals*

The dynamic range of tropospheric lidar signals is very high (at least 4 orders of magnitude). In the near range the signal is extremely high, while in the far range it is extremely weak. In both of these extreme conditions, a good signal to noise ratio and linearity between light intensity and measured signal are required. Lidar signals acquired in analog mode have a high signal to noise ratio in the near range, but a low signal to noise ratio and possible distortions in the far range. On the other hand, lidar signals acquired in photon counting mode have a very good signal to noise ratio in the far range, but they are problematic for very high count rates, that occurs in the near range. In these conditions, the signals in photon counting mode lose their linearity due to the dead time and the greater the count rate, the more difficult to correct for this effect.
Given the complementarity between analog signals and photon counting signals, it is possible to extend the detectable dynamic range of lidar, by appropriately combining the analog signal with that in photon counting mode, so as the “main” signal of lidar channel is the signal in photon counting mode and the corresponding analog signal becomes an extension in the near range of the signal in photon counting mode. This operation is called gluing between the analog signal and the signal in photon counting mode. This gluing is performed by the following steps:

1) Identifying a minimum range q_{min} above which non linear effects in the photon counting signal, due to the dead time, are absent or corrected in reliable way. (Typically, q_{min} corresponds to a count rate of about 20-30MHz in the photon counting signal).

2) Identifying a maximum range q_{max} below which distortions in the analog signal are neglected. This maximum range corresponds to a value of the analog signal *of* V_{fs}/K, where V_{fs} is the maximum acquisition value and *K is* a factor depending on the quality of the ADC. *(*Typically K ranges from 1000 to 20000).

3) If q_{max} is higher than q_{min}, analog and photon counting signals can be glued; otherwise the procedure is stopped.

4) A linear fit of photon counting signal and of analog signal is performed in the interval $[q_{min}, q_{max} - dq,]$with dq= 0.

5) If the coefficients of linear fits in the previous step are consistent, within their experimental errors, the procedure goes to the next step; otherwise, it returns to the step 4) with dq=q, where q is a multiple of the raw spatial resolution of lidar signals.

6) The analog signal is scaled on the photon counting signal by a linear fit in the interval $[q_{min},q_{max}-dq]$

7) The gluing point is identified in the interval $[q_{min},q_{max}-dq]$ as the point for which the difference between the analog signal and photon counting signal is minimum.

8) Finally, the glued signal is formed by the scaled analog signal, for ranges below the gluing point, and by the photon counting signal for ranges above the gluing point.

Analysis and interpretation of optical properties

In this section the algorithms for the retrieval of particle optical properties are described. These algorithms use the pre-processed and corrected lidar signals of the previous section as input data.

- *Particle backscattering coefficient*

The profiles of particle backscattering coefficient $\beta_{\lambda_L}^{par}(r)$ at the laser wavelength λ_L =532nm is retrieved using an iterative method (Di Girolamo et al., 1999). The particle backscattering coefficient in the i-th iteration step is calculated by the following equation:

$$\beta_{\lambda_L,i}^{par}(r) = \left(\frac{P_{\lambda_L}(r)K_{\lambda_L,i}}{P_{\lambda_L,i}^{mol}(r)} - 1\right)\beta_{\lambda_L}^{mol}(r)$$

where: $P_{\lambda_L}(r)$ is the power of the pre-processed lidar signal at wavelength λ_L , depending on the distance r from the laser source; $\beta_{\lambda_L}^{mol}(r)$ is the molecular backscattering coefficient at the laser wavelength λ_L, calculated from Rayleigh theory and atmospheric molecular density profiles retrieved from models or radiosonde measurements; $\mathrm{P}_{\lambda_L,\mathrm{i}}^{\mathrm{mol}}(\mathrm{r})$ is an estimated molecular signal, expressed as:

$$P_{\lambda_L,i}^{mol}(r) = \beta_{\lambda_L}^{mol}(r)exp\left(-2\int_0^r S_{\lambda_L}(r')\beta_{\lambda_L,i-1}^{par}(r')dr'\right)$$

where $S_{\lambda_L}(r)$ is an assumed particle lidar ratio profile; the particle lidar ratio is defined as the ratio of the particle extinction coefficient and the particle backscattering coefficient:

$$S_{\lambda_L}(r) = \frac{\alpha_{\lambda_L}^{par}(r)}{\beta_{\lambda_L}^{par}(r)}$$

$K_{\lambda_L,i}$ is a calibration factor and can be determined in an aerosol-free region r_{ref} :

$$K_{\lambda_L,i} = \frac{P_{\lambda_L,i}^{mol}(r_{ref})}{P_{\lambda_L}(r_{ref})}$$

In an initial step, the molecular signal $P_{\lambda_L,0}^{mol}(r)$ is estimated with the assumption $\beta_{\lambda_L}^{par}(r) = 0$ and is then used to derive an initial value of $\beta_{\lambda_L,0}^{par}(r)$. In the following iteration step i, the backscatter coefficient $\beta_{\lambda_L,i}^{par}(r)$ is calculated from a molecular signal which is estimated from the previous backscatter profile $\beta_{\lambda_L,i-1}^{par}(r)$. This procedure is repeated until the difference between $\beta_{\lambda_L,i}^{par}(r)$ and $\beta_{\lambda_L,i-1}^{par}(r)$ is smaller than a certain threshold.

- *Particle linear depolarization ratio*

The profile of particle linear depolarization ratio $\delta^{par}(r)$ is derived from the following equation (Freudenthaler et al., 2009):

$$\delta^{par}(r) = \frac{\beta_{\perp}^{par}(r)}{\beta_{\parallel}^{par}(r)} = \frac{(1+\delta^m)\delta^V(r)R(r) - (1+\delta^V(r))\delta^m}{(1+\delta^m)R(r) - (1+\delta^V(r))}$$

where $\beta_{\perp}^{par}(r)$ is the particle volume backscattering coefficient from the range r, with a polarization perpendicular to the polarization of the laser source; $\beta_{\parallel}^{par}(z)$ is the particle volume backscattering coefficient from the range r, with a polarization parallel to the polarization of the laser source; $\delta^V(r)$ is the volume depolarization ratio, defined and calculated during the calibration of polarization channels; δ^m is the linear depolarization ratio of air molecules, that can be calculated by using Rayleigh theory:

$$\delta^m(r) = \frac{\beta_{\perp}^{mol}(r)}{\beta_{\parallel}^{mol}(r)}$$

Finally $R(r)$ is the backscatter ratio, i.e the ratio of the total backscattering coefficient to the molecular component, that can be calculated from particle backscattering coefficient $\beta_{\lambda_L}^{par}(r)$:

$$R(z) = \frac{\beta_{\lambda_L}^{par}(r) + \beta_{\lambda_L}^{mol}(r)}{\beta_{\lambda_L}^{mol}(r)} = 1 + \frac{\beta_{\lambda_L}^{par}(r)}{\beta_{\lambda_L}^{mol}(r)}$$

The particle backscattering coefficient $\beta_{\lambda}^{par}(r)$ at wavelength λ is a measure of the scattering in the backward direction (i.e. towards the incident direction, at an scattering angle of 180°) for the light encountering the atmospheric aerosol or cloud particles.

The particle extinction coefficient $\alpha_\lambda^{par}(r) = \beta_\lambda^{par}(r) S_\lambda(r)$ at wavelength λ is a measure of attenuation of the light passing through the atmosphere due to the scattering and absorption by aerosol or cloud particles. The extinction coefficient is the sum of the absorption coefficient and the scattering coefficient.
The optical depth τ of an aerosol or cloudy layer is defined as the integral of the particle extinction coefficient over the range interval from the base to the top of the layer:

$$\tau_{layer} = \int_{base}^{top} \alpha^{par}(r)dr$$

The column optical depth is also a variable often used to describe aerosol and clouds properties over the full atmospheric column, and it is defined as the integral of the particle extinction coefficient from the ground to the top of the atmosphere (TOA):

$$\tau_{column} = \int_{0}^{TOA} \alpha^{par}(r)dr$$

This definition allows to include also contribution from stratospheric aerosol if present.
Backscattering coefficient, extinction coefficient and optical depth of atmospheric particles represent the extensive optical properties of aerosol and clouds, depending on both the amount and the nature (size, shape and composition) of atmospheric particles. The particle lidar ratio $S_\lambda(r)$ is an intensive optical property of aerosol and clouds, depending only on the nature of particles, but not on their concentration. For example, for clouds with droplet size distributions with median volume diameters in the range 5-50 μm, the value of lidar ratio at infrared wavelengths is approximately constant with a value of 18.75 sr (O'Connor et al., 2004).
The particle linear depolarization ratio $\delta^{par}(r)$ is an important intensive optical property, providing information on the shape or sphericity of atmospheric particles. Spherical particles, such as water droplets, are characterized by very low values of $\delta^{par}(r)$, while particles with non-spherical shape have higher values of $\delta^{par}(r)$, that increases as much as their shape deviates from sphericity. As a consequence, particle linear depolarization ratio allows to discriminate between water droplets and ice crystals in clouds, so identifying water phase in clouds, like cirrus and mixed–phase clouds. Moreover, particle linear depolarization ratio allows to distinguish different types of aerosols. For example, it is possible to discriminate between desert dust, mostly characterized by non-spherical and irregular particles, and marine aerosols, with more regular and spherical shape.
The lidar system allows to characterize the aerosol layers in troposphere by the profiles of their intensive and extensive optical properties, their optical depth and spatial structure. Furthermore, by algorithms based on threshold values of the optical parameters from literature, it is possible to discriminate between aerosols and clouds, identify the cloud base position and measure the cloud fraction. Finally, for optically thin clouds it is possible to calculate the profiles of their intensive and extensive optical properties, their optical depth and spatial structure.

References

Bucholtz, A., Rayleigh-scattering calculations for the terrestrial atmosphere, Appl. Opt. Vol. 34, N. 15, pp. 2765-2773 (1995).

Di Girolamo, P., P. F. Ambrico, A. Amodeo, A. Boselli, G. Pappalardo, and N. Spinelli, "Aerosol observations by lidar in the nocturnal boundary layer", Appl. Opt., 38 (21), 4585–4595, 1999.

Freudenthaler, V., Esselborn, M., Wiegner, M., Heese, B., Tesche, M., Ansmann, A., Müller, D., Althausen, D., Wirth, M., Fix, A., Ehret, G., Knippertz, P., Toledano, C., Gasteiger, J., Garhammer, M. And Seefeldner, M., Depolarization ratio profiling at several wavelengths in pure Saharan dust during SAMUM 2006. Tellus B, 61: 165–179. doi: 10.1111/j.1600-0889.2008.00396.x, (2009).

Madonna, F., Amodeo, A., Boselli, A., Cornacchia, C., Cuomo, V., D'Amico, G., Giunta, A., Mona, L., and Pappalardo, G.: CIAO: the CNR-IMAA advanced observatory for atmospheric research, Atmos. Meas. Tech., 4, 1191-1208, doi:10.5194/amt-4-1191-2011, 2011.

Miles R. et al, Laser Rayleigh scattering, Meas. Sci. Technol. , 12, R33-R51 (2001).

O'Connor, E.J., A.J. Illingworth and R. J. Hogan, "A technique for autocalibration of cloud lidar", J. Atmos. Ocean. Tech., 21(5), 777- 778, 2004

Pappalardo, G., Amodeo, A., Apituley, A., Comeron, A., Freudenthaler, V., Linné, H., Ansmann, A., Bösenberg, J., D'Amico, G., Mattis, I., Mona, L., Wandinger, U., Amiridis, V., Alados-Arboledas, L., Nicolae, D., and Wiegner, M.: EARLINET: towards an advanced sustainable European aerosol lidar network, Atmos. Meas. Tech., 7, 2389-2409, doi:10.5194/amt-7-2389-2014, 2014.